

See discussions, stats, and author profiles for this publication at: <https://www.researchgate.net/publication/221624594>

# Fully automatic and fast segmentation of the femur bone from 3D-CT images with no shape prior

**Conference Paper** in *Proceedings / IEEE International Symposium on Biomedical Imaging: from nano to macro. IEEE International Symposium on Biomedical Imaging* · March 2011

DOI: 10.1109/ISBI.2011.5872823 · Source: DBLP

---

CITATIONS

72

---

READS

838

3 authors, including:



**Gábor Székely**

ETH Zurich

331 PUBLICATIONS 12,466 CITATIONS

SEE PROFILE



**Remi Blanc**

Thermo Fisher Scientific

27 PUBLICATIONS 807 CITATIONS

SEE PROFILE

Some of the authors of this publication are also working on these related projects:



Microrobots for biomedical applications [View project](#)



Medical Robotics Sensing and Control [View project](#)

# FULLY AUTOMATIC AND FAST SEGMENTATION OF THE FEMUR BONE FROM 3D-CT IMAGES WITH NO SHAPE PRIOR

Marcel Krčah<sup>1,2</sup>    Gábor Székely<sup>1</sup>    Rémi Blanc<sup>1</sup>

<sup>1</sup> Computer Vision Laboratory, ETH Zurich, Zurich, Switzerland

<sup>2</sup> Faculty of Mathematics and Physics, Charles University, Prague, Czech Republic

## ABSTRACT

Statistical shape and intensity modelling have been subject to an increasing interest within the past decade. However, construction of such models requires large number of segmented examples. Accurate and automatic segmentation techniques that do not require any explicit prior model are therefore of high interest. We propose a fully-automatic method for segmenting the femur in 3D Computed Tomography (CT) volumes, based on graph-cuts and a bone boundary enhancement filter analysing the second-order local structure. The presented technique is evaluated in large-scale experiments, conducted on 197 femur samples, and compared to other three automatic bone segmentation methods. Our approach achieved accurate femur segmentation in 81% of cases without any shape prior or user interaction.

*Index Terms*— CT, bone segmentation, graph-cuts, sheetness measure, femur

## 1. INTRODUCTION

Statistical shape and intensity modeling have been subject to an increasing interest within the past decade in a wide variety of applications [1]. Particularly in the domain of orthopaedics, they are of high interest for intra-operative guidance, reconstructive surgery or implant design. However, learning such models requires that a large number of examples are available and pre-processed. Segmentation, in particular, remains a serious bottleneck in this context and manual processing is common practice. Accurate and automatic segmentation methods requiring no explicit prior model are therefore of high interest.

Segmentation of long bones in CT images is a relatively simple task, due to high contrast between the thick, strongly attenuating cortical layer and the encasing low-intensity soft tissue. However, segmentation still remains a challenge in the joint epiphysis areas, where the cortical layer becomes much thinner and the contrast between the cancellous bone and soft tissues is less pronounced. Additionally, the inter-bone space

becomes very narrow and partial volume effects result in very weak contrast in these regions (Fig. 1a).

As pointed out in [2], despite several years of active research, bone segmentation remains in several aspects an open problem. Intensity-based methods, such as (local) binary thresholding or region growing, tend to produce discontinuous contours and “leakages” to soft-tissues or adjacent bones. Active contour models, such as snakes or level-set methods [3], are sensitive to initialization and are of limited use in areas of low gradient. More recently, the graph-cut framework [4, 5] has shown to provide an elegant and efficient approach for segmentation. It was applied to bone segmentation, e.g. in [6], with promising results. We extend this approach to a fully 3D formulation. In particular, we propose new energy terms for the graph-cut which utilize the sheetness measure inspired by [7]. A post-processing step is also presented for the automatic separation of adjacent bones.

Details of the proposed method are given in Section 2. In Section 3, we evaluate the method on a database of 197 cases, for which both original CTs and manual segmentations were available, and compare it with three other automatic methods. Section 4 concludes the paper.

## 2. OVERVIEW OF THE GRAPH-CUT SEGMENTATION PROCEDURE

The proposed procedure, illustrated in Fig. 1, is based on Boykov and Jolly’s graph-cut segmentation framework [5], briefly presented in Section 2.1. To segment all bone tissues in the input 3D CT volume  $\mathcal{I} : \Omega \rightarrow R$ , the graph-cut relying on the terms described in Sections 2.2 and 2.3 is employed.

The output of the graph-cut is a binary volume with all bone-voxels labelled, as depicted in Fig. 1d. Due to narrow inter-bone spacing, the procedure is often not sufficient to perfectly segment the femur as leakage to adjacent bones (pelvis, tibia and patella) may occur. Experiments have shown that in such cases adjacent bones are connected to the femur generally by only a few voxels. Individual bones are therefore identified in a post-processing step, described in Section 2.4, and the femur is determined as the largest connected component in the final volume.

---

This work is part of the Virtual Skeleton Database project, NCCR Co-Me (<http://co-me.ch>), funded by the Swiss National Science Foundation.

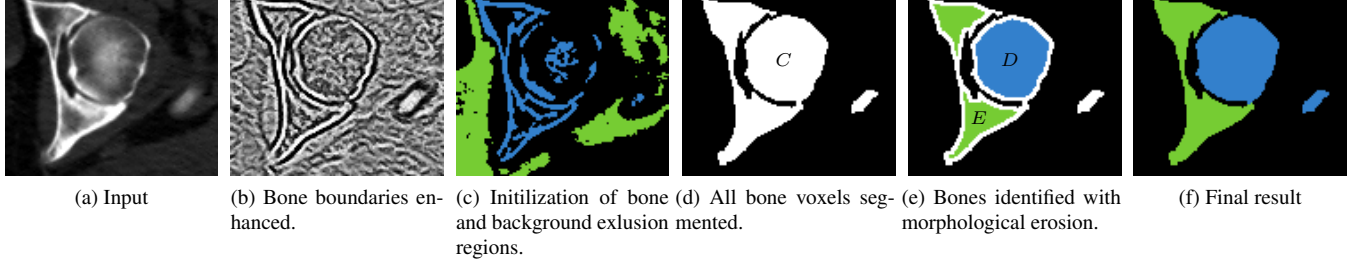


**Fig. 1:** The proposed method illustrated on an axial slice of the acetabulofemoral joint of the input 3D CT image.

## 2.1. The Graph-Cut Framework

The graph-cut [5] is an energy-minimization segmentation framework based on combinatorial graph theory. In general, the method requires to define two components of a cost function: the *per-pixel* and the *boundary* term. The *per-pixel* term  $R_p(A_p) : \Omega \times \{0, 1\} \rightarrow R_0^+$  specifies a penalty for assigning the label  $A_p$  to the voxel  $p$ . The *boundary* term  $B(p, q) : \mathcal{N} \rightarrow R_0^+$  defines a penalty for classifying the voxel  $p$  as an object and the voxel  $q$  as background, within a symmetric neighborhood system  $\mathcal{N} \subset \Omega^2$ .

The method finds a binary labelling  $A$  as a global minimum of an energy function  $E(A)$  defined as:

$$E(A) = \sum_{p \in \Omega} R_p(A_p) + \lambda \sum_{(p,q) \in \mathcal{N}} \delta(A_p, A_q) B(p, q), \quad (1)$$

where  $\delta$  is the Kronecker delta and  $\lambda$  defines the relative importance of the per-pixel and the boundary term.

## 2.2. The Boundary Term

The boundary term encourages spatial coherence within the object and within the background, i.e. the penalty is low on boundaries and high elsewhere. A boundary term based only on intensities leads to unsatisfactory results due to weak bone edges and poor contrast in joint regions. The contrast at bone boundaries is therefore enhanced by successively applying two filters:

First, the input image is enhanced by the unsharp masking, defined as  $\mathcal{I}^U = \mathcal{I} + k(\mathcal{I} - \mathcal{I} \star G_s)$ , where  $\star$  denotes convolution,  $G_s$  is a Gaussian kernel with variance  $s^2$  and  $k$  denotes a scaling constant. Subsequently, the image is processed with a *sheetness* filter, inspired by [7]. For each voxel of  $\mathcal{I}^U$ , a sheetness score is computed from the eigenvalues  $|\lambda_1| \leq |\lambda_2| \leq |\lambda_3|$  of the local Hessian matrix as:

$$S_\sigma(x) = -\text{sgn}(\lambda_3) \exp \left\{ -\frac{R_{sheet}^2}{\alpha^2} \right\} \exp \left\{ -\frac{R_{tube}^2}{\beta^2} \right\} \left( 1 - \exp \left\{ -\frac{R_{noise}^2}{\gamma^2} \right\} \right),$$

with  $R_{sheet} = |\lambda_2|/|\lambda_3|$ ,  $R_{tube} = |\lambda_1|/(|\lambda_2||\lambda_3|)$  and  $R_{noise} = (|\lambda_1| + |\lambda_2| + |\lambda_3|)/T$ , where  $T$  denotes average trace of the Hessian at each image voxel. In order to

increase the contrast at bone boundaries, we have incorporated the sign of the largest eigenvalue into the sheetness score. Finally, the robustness of the sheetness is improved through a multi-scale implementation, by computing the Hessian matrix at different scales  $\Sigma$  and retaining, for each voxel, the sheetness response corresponding to the highest absolute value.

The output of these filters, denoted  $S$ , enhances bone boundaries, especially at joint areas (Fig. 1b). We employ it for defining the boundary term of the graph-cut cost function (1):

$$B(p, q) \propto \begin{cases} \exp \left\{ -\frac{|S(p) - S(q)|}{\sigma_s} \right\} & \text{for } S(p) \geq S(q), \\ 1 & \text{otherwise,} \end{cases}$$

where  $\sigma_s$  is a constant scaling parameter. This definition encourages boundaries in regions with abrupt variations of the sheetness value. We exploit directed edges of the underlying combinatorial graph (see [5]) to obtain more precise bone boundaries by favoring transitions from bone to background in regions with decreasing sheetness score.

## 2.3. The Per-Pixel Term

The per-pixel term  $R_p(A_p)$  reflects the penalty for assigning the voxel  $p$  the label  $A_p$ . The cost should be therefore low if (a)  $p$  belongs to a bone and  $A_p = 1$  or if (b)  $p$  belongs to background and  $A_p = 0$ ; otherwise the cost should be high. Weak bone boundaries, narrow inter-bone space and low intensities in the trabecular bone make image intensity alone a relatively poor feature for discriminating bone from background. Nevertheless, exclusion regions  $E_{-bkg}$  and  $E_{-bone}$  (Fig. 1c) can safely be estimated as:

$$E_{-bkg} = \{x \in \Omega | \mathcal{I}(x) \geq 400 \text{ HU} \wedge S(x) > 0\},$$

$$E_{-bone} = \text{lcc}(\{x \in \Omega | \mathcal{I}(x) < -50 \text{ HU}\}),$$

where  $\text{lcc}$  denotes the largest connected component of the binary argument. The term  $\mathcal{I}(x) \geq 400 \text{ HU}$  selects high-intensity voxels present mostly in cortical bone while  $S(x) > 0$  discards soft-tissue voxels in narrow inter-bone areas. The term  $\{x | \mathcal{I}(x) < -50 \text{ HU}\}$  retains mostly fat and air voxels of low intensity values, rarely encountered in the bone interior.

The per-pixel term of the graph-cut cost function (1) is defined as

$$R_p(A_p) \propto \begin{cases} 1 & \text{if } A_p = \text{"bone"} \text{ and } p \in E_{-bone}, \\ 1 & \text{if } A_p = \text{"bkg"} \text{ and } p \in E_{-bkg}, \\ 0 & \text{otherwise.} \end{cases}$$

This initial classification can be considered as the initialization of the graph-cut segmentation (Fig. 1c). Since its value is 0 for all voxels outside  $E_{-bkg} \cap E_{-bone}$ , it is the boundary term that arbitrates on the classification of these voxels.

#### 2.4. Postprocessing: Bone Separation

To separate neighboring bones, a morphological erosion with a spherical element of radius  $R$  is applied to the binary image (Fig. 1e). If the erosion divides a component  $C \subset \Omega$  into two subcomponents  $D, E \subset C$ , a bottleneck has to be present in  $C$ . Our goal is to find disjoint sets  $D', E' \subset \Omega$  such that  $D' \cup E' = C, D \subset D', E \subset E'$  and that the number of voxels on the boundary between both sets is minimal. To accurately find  $D', E'$ , a simplified graph-cut is employed on the image part  $C$ . The hard-constraints  $D \subset D', E \subset E'$  are imposed on the classification via the per-pixel term:

$$\forall p \in C : R_p(A_p) = \begin{cases} \infty & \text{if } A_p = \text{"D"} \text{ and } p \in E, \\ \infty & \text{if } A_p = \text{"E"} \text{ and } p \in D, \\ 0 & \text{otherwise.} \end{cases}$$

The boundary term  $B(p, q) = B(q, p) = 1$  encourages minimal boundary between  $D'$  and  $E'$ . This procedure can be employed to either segment all bones in the image by assigning them different labels or to extract only one of them (Fig. 1f).

### 3. EXPERIMENTS AND RESULTS

Experiments were conducted on 197 CT volumes, cropped around the femur, with image intensities expressed as Hounsfield units. The volume spacing ranged from 0.6 to 1.17mm in-plane and from 0.8 to 1.25mm inter-slice.

For all datasets, a manual segmentation by a medical expert was available and served as a reference for quantitative evaluations. For each sample, we measured the True Positive Rate  $TPR = TP/(TP+FN)$ , False Positive Rate  $FPR = FP/(FP+TN)$  and the Hausdorff distance (HD) between the estimated and the reference surfaces. Additionally, the time to process and memory consumption were recorded.

#### 3.1. Implementation

The proposed method was implemented in C++ using the ITK library (<http://itk.org>) and Boykov-Kolmogorov's max-flow library [4] for efficient computation of the graph-cut. The following parameters were manually selected:  $\lambda = 5, k =$

$10, s = 1, \alpha = \beta = 0.5, \gamma = 0.25, \Sigma = \{0.75, 1.0\}, \sigma_s = 0.2, R = 3$ , and kept constant for all datasets.

We compared our method to three existing fully-automatic 3D-based bone segmentation schemes: gradient-based geometric active contour (GeomAC) [3], Zhang iterative adaptive thresholding (ZIAT) [8] and an intensity-based graph-cut method (IBGC). For GeomAC, the ITK implementation was employed with the initial level-set initialized as the signed distance of the binary image  $E_{-bone}$ , propagation parameter 5.0, curvature parameter 1.0 and max. number of iterations 400. The ZIAT method was implemented with a window size 15x15x3px and initial threshold value 70. For IBGC, the graph-cut algorithm was employed with the following components:  $R_p(\text{bone}) = 1$  for  $p \in E_{-bone}$ , 0 otherwise;  $R_p(\text{bkg}) = 1$  for  $\mathcal{I}(p) > 500$  HU, 0 otherwise;  $B(p, q) = B(q, p) = \exp\{|\mathcal{I}(p) - \mathcal{I}(q)|/100\}$ .

#### 3.2. Results

The results (Fig. 2 and 3) show that all tested approaches, except ZIAT, are able to correctly discriminate the true femur voxels with satisfactory precision ( $TPR > 0.85$ ). Due to the low contrast in narrow inter-bone channels and weak bone boundaries, leakage (GeomAC, IBGC, ZIAT) and contour discontinuity (ZIAT) always occurred in segmentations from these three methods. None of them could separate the femur accurately (HD > 5cm), nor segment the challenging weak bone contours (visual evaluation).

Conversely, our approach is clearly superior in detecting bone boundaries in narrow inter-bone regions and in suppressing leakage into adjacent bones. The proposed method correctly segmented and separated the femur from adjacent bones ( $TPR > 0.85, FPR < 0.001, HD < 8\text{mm}$ ) in 81% of the cases, with average HD of 5.4mm within this set. The

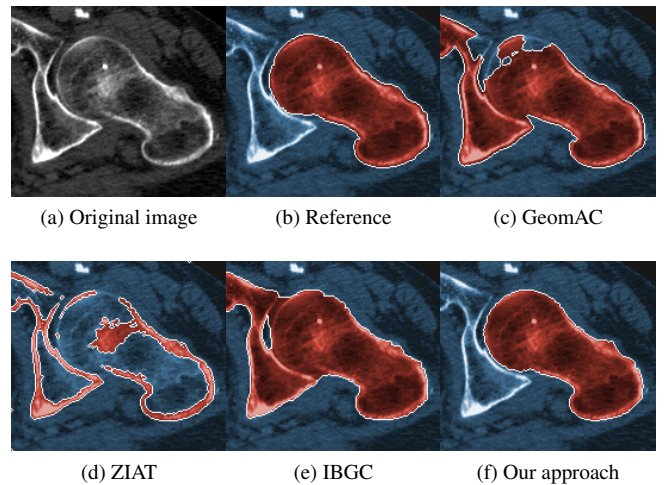


**Fig. 2:** Segmentation results of four tested methods illustrated on axial slice of acetabulofemoral joint.

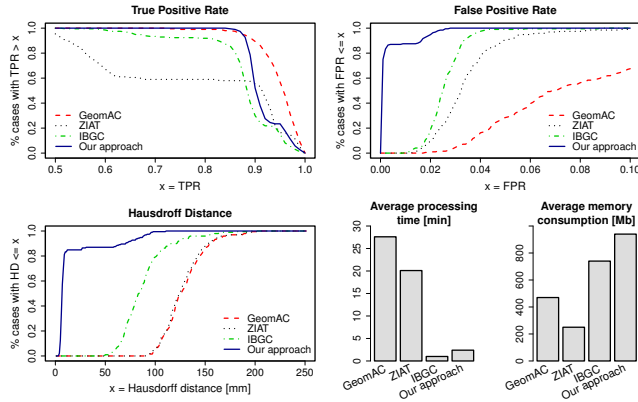


**Fig. 3:** Results of experiments conducted on 197 femoral samples.

postprocessing procedure (Section 2.4) separated the femur from at least one neighboring bone in 57% of cases.

Graph-cut-based approaches have also proven to be much faster (only a few minutes per dataset), albeit consuming more memory. However, the high memory requirements can be decreased by employing alternative graph-cut algorithms (e.g. [9]).

#### 4. CONCLUSION

We have presented a fully automatic method for segmenting the femur from 3D-CT images, based on the graph-cut algorithm and a novel bone boundary enhancement filter. The strengths of the modified sheetness score combined with the automatic bone separator have been proven in large-scale experiments conducted on 197 femur CT volumes; the procedure segmented the femur accurately in 81% of cases. The method was also compared to other existing fully-automatic solutions; however, all of them require manual postprocessing in order to achieve satisfactory results.

As no explicit priors are required, the proposed method is also suitable for segmenting other bones in CT. Preliminary experiments on forearms, (toothless) mandibles and wrists showed promising results (Fig. 4) without any parameter tuning.

Future work aims at embedding this automatic segmentation framework into a statistical model generation approach, by iteratively improving the model and refining the segmentations.

#### 5. REFERENCES

[1] Tobias Heimann and Hans-Peter Meinzer, “Statistical shape models for 3d medical image segmentation: A review,” *Medical Image Analysis*, vol. 13, no. 4, pp. 543 – 563, 2009.

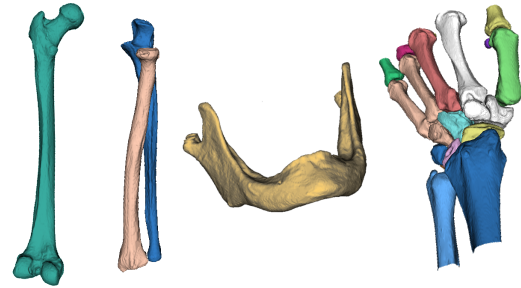


**Fig. 4:** 3D models generated from an automatically segmented femur, radius and ulna, mandible, carpal bones (from left to right).

[2] L.I. Wang, M. Greenspan, and R. Ellis, “Validation of bone segmentation and improved 3-D registration using contour coherency in CT data,” *IEEE transactions on medical imaging*, vol. 25, no. 3, pp. 324, 2006.

[3] R. Malladi, J.A. Sethian, B.C. Vemuri, et al., “Shape modeling with front propagation: A level set approach,” *IEEE Transactions on Pattern Analysis and Machine Intelligence*, vol. 17, no. 2, pp. 158–175, 1995.

[4] Y. Boykov and V. Kolmogorov, “An experimental comparison of min-cut/max-flow algorithms for energy minimization in vision,” *IEEE Transactions on Pattern Analysis and Machine Intelligence*, pp. 1124–1137, 2004.

[5] Y. Boykov and G. Funka-Lea, “Graph cuts and efficient nd image segmentation,” *International Journal of Computer Vision*, vol. 70, no. 2, pp. 109–131, 2006.

[6] P. Furnstahl, T. Fuchs, A. Schweizer, L. Nagy, G. Székely, and M. Harders, “Automatic and robust forearm segmentation using graph cuts,” *Biomedical Imaging: From Nano to Macro*, 2008.

[7] M. Descoteaux, M. Audette, K. Chinzei, and K. Siddiqi, “Bone enhancement filtering: Application to sinus bone segmentation and simulation of pituitary surgery,” *Lecture Notes in Computer Science*, vol. 3749, pp. 9, 2005.

[8] J. Zhang, C.H. Yan, C.K. Chui, and S.H. Ong, “Fast segmentation of bone in CT images using 3D adaptive thresholding,” *Computers in Biology and Medicine*, vol. 40, no. 2, pp. 231–236, 2010.

[9] A. Delong and Y. Boykov, “A scalable graph-cut algorithm for nd grids,” in *Computer Vision and Pattern Recognition, 2008. CVPR 2008. IEEE Conference on*. IEEE, 2008, pp. 1–8.